

Minerva Access is the Institutional Repository of The University of Melbourne

Author/s:

Ren, JM;Subbiah, J;Zhang, B;Ishitake, K;Satoh, K;Kamigaito, M;Qiao, GG;Wong, EHH;Wong, WWH

Title:

Fullerene peapod nanoparticles as an organic semiconductor-electrode interface layer

Date:

2016-01-01

Citation:

Ren, J. M., Subbiah, J., Zhang, B., Ishitake, K., Satoh, K., Kamigaito, M., Qiao, G. G., Wong, E. H. H. & Wong, W. W. H. (2016). Fullerene peapod nanoparticles as an organic semiconductor-electrode interface layer. *Chemical Communications*, 52 (16), pp.3356-3359. <https://doi.org/10.1039/c5cc10444k>.

Persistent Link:

<https://hdl.handle.net/11343/220179>

Fullerene Peapod Nanoparticles as Organic Semiconductor-Electrode Interface Layer

Received 00th January 20xx,
Accepted 00th January 20xx

Jing M. Ren,^{†a} Jegadesan Subbiah,^{†b} Bolong Zhang,^b Kenji Ishitake,^c Kotaro Satoh,^c Masami Kamigaito,^c Greg G. Qiao,^{*a} Edgar H. H. Wong,^{*†a} and Wallace W. H. Wong^{*b}

DOI: 10.1039/x0xx00000x

www.rsc.org/

Syndiotactic poly(methyl methacrylate) bottlebrush polymer has been shown to complex C₆₀ fullerene and assemble into nanoparticles that can be dispersed in polar organic solvents. This composite material was used as the electrode interlayer in organic solar cell (OSC) devices leading to enhancements in device performance.

Flexible electronics are part of the next wave of technology that promise light-weight, conformable, integrated devices that can be produced at low-cost.¹ The development of high performance solution-processed functional materials is a key area of research in this important technology trend. Fullerenes, a class of highly symmetric cage-shaped molecules comprised of only carbon atoms, are amongst one of the most widely used materials in organic electronic thin films because of their reversible reduction behaviour² and good electron transport properties.³ However, pure fullerenes are only sparingly soluble in solvents, and generally modified fullerene derivatives are used instead to improve miscibility/solubility for thin film processing.⁴ The ability to disperse fullerene molecules effectively is crucial towards controlling the film morphology and consequently the device performance.⁵ In spite of the availability of fullerene derivatives, morphological control in thin films remains challenging.⁶

Recently, Yashima and co-workers reported a versatile method to encapsulate unmodified fullerene C₆₀ (or C₇₀) into the helical cavities of syndiotactic poly(methyl methacrylate) (*st*-PMMA), forming distinct one-dimensional (1D) arrays of fullerenes within the *st*-PMMA scaffold.⁷ These supramolecular complexes, termed fullerene molecular peapods, have several

advantages compared to conventional fullerene derivatives: i) the *st*-PMMA scaffold is a commodity plastic and is easy to process and produce on a large scale; ii) fullerene peapods disperse very efficiently in solutions due to the excellent compatibility of PMMA with many organic solvents and prevent phase separation when deposited as thin films; iii) the photophysical properties of the fullerenes are largely retained and differ from those of the fullerene derivatives; and iv) unmodified fullerenes are cheaper compared to their derivatives. Despite the many interesting properties and potential of these fullerene peapods, the application in electronic materials is still relatively new.^{7a}

Encouraged by the work from the Yashima group,^{7,8} we herein describe the preparation of a novel *st*-PMMA bottlebrush (*st*-PMMA-BB) polymer with encapsulated C₆₀, termed fullerene peapod nanoparticle (FPN), as organic semiconductor-electrode interface layer (Scheme 1). By encasing native C₆₀ within the *st*-PMMA-BB, the formed FPNs have excellent solubility in organic solvents and can be easily processed into thin films. In addition, bulk-heterojunction (BHJ) solar cells made using FPN films as the solar cell-electrode interface layer yield higher power conversion efficiency (PCE) (ca. 10-30% more) compared to those made with a ZnO interface layer. This study crucially demonstrates the advantage of macromolecular engineering in improving the performance of organic electronic materials. In the following, the synthetic strategy leading to the formation of FPNs is thoroughly elucidated, while various BHJ solar cells have been fabricated to confirm the efficacy of FPNs as an effective interface layer.

The *st*-PMMA-BB bottlebrush polymer was prepared via ring-opening metathesis polymerization (ROMP)⁹ using *exo*-norbornene chain-end functionalized syndiotactic poly(methyl methacrylate) (*st*-PMMA-NB) as macromonomer (Scheme 1). Firstly, the polymerization of the macromonomer was achieved via stereospecific living radical polymerization (SLRP).¹⁰ The SLRP technique afforded polymer products with simultaneous control over their molecular weight (MW) and tacticity (Scheme S1, Supporting Information).

^a Department of Chemical and Biomolecular Engineering, The University of Melbourne, Parkville, Victoria 3010, Australia.

E mail: gregghq@unimelb.edu.au; edgar.wong@unsw.edu.au

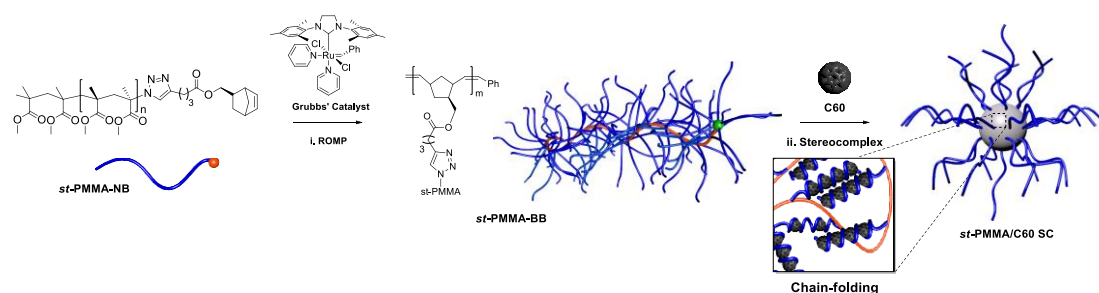
^b School of Chemistry, Bio21 Institute, The University of Melbourne, 30 Flemington Road, Parkville, Victoria 3010, Australia. E mail: wwhwong@unimelb.edu.au

^c Department of Applied Chemistry, Graduate School of Engineering, Nagoya University, Furo-cho, Chikusa-ku, Nagoya 464-8603, Japan.

† Present address: Centre for Advanced Macromolecular Design and Australian Centre for Nanomedicine, School of Chemical Engineering, The University of New South Wales, Sydney, NSW 2052, Australia.

† These authors contributed equally to this study.

Electronic Supplementary Information (ESI) available: [Experimental methods and full characterization data]. See DOI: 10.1039/x0xx00000x



Scheme 1. Schematics for (i) the synthesis of syndiotactic poly(methyl methacrylate) bottlebrush polymer (*st*-PMMA-BB) via ring-opening metathesis polymerization (ROMP), and (ii) the preparation of FPN *st*-PMMA-BB/C₆₀ stereocomplex (SC) via stereocomplexation.

Although SLRP offers a lower level of syndiotacticity control than anionic polymerization because of the less regulated stereospecific propagation environment,¹¹ a well-defined linear *st*-PMMA with sufficient degree of tacticity to form PMMA stereocomplex ($rr = 74\%$)^{8c,d} was achieved nonetheless. After modifying the ω -chain end from chloride to azide, the ROMP-polymerizable norbornene functionality was installed *via* classical 'click' chemistry to afford *st*-PMMA-NB (with number-average MW (M_n) = 5.5 kDa, dispersity (\mathcal{D}) = 1.10, $mm/mr/rr$ (%) = 1.5/24.5/74.0, and ω -end group functionality ($F(\omega)$) = 0.88, Figure S1, SI). Noteworthy, as the *exo*-isomer of norbornene is more reactive towards ROMP than the *endo*-isomer,¹¹ an *exo*-norbornene derivative was specifically designed to introduce the polymerizable functionality, allowing for the subsequent rapid and highly-efficient formation of well-defined bottlebrush polymer *via* a grafting-through approach.¹²

The *st*-PMMA-BB was successfully synthesized *via* the ROMP of *st*-PMMA-NB initiated by the highly active pyridine-modified 2nd Generation Grubbs Catalyst.⁹ The GPC differential refractive index (DRI) traces (Figure 1a) showed near-quantitative conversion (> 90%) of *st*-PMMA-NB into a high MW species ($M_n = 183.7$ kDa and $\mathcal{D} = 1.38$), indicating the successful formation of *st*-PMMA-BB. Unconverted macromonomers were removed *via* preparative GPC, which were characterized *via* ¹H NMR spectroscopic analysis and found to possess no polymerizable terminus. To accurately determine the MW of *st*-PMMA-BB and account for the structural deviation of the bottlebrush polymer from the GPC calibration standards (i.e., linear PMMAs), GPC couple with a multi-angle laser light scattering detector (GPC-MALLS) – a technique which allows for the determination of the absolute MW independent of the polymer architecture – was used to re-characterize *st*-PMMA-BB and it was found to have $M_n(\text{MALS}) = 815.9$ kDa and $\mathcal{D} = 1.12$, which translates to *ca.* 148 *st*-PMMA side-chains per bottlebrush polymer on average (i.e., $m = 148$). The ¹H NMR spectrum of *st*-PMMA-BB (Figure 1b) displayed characteristic resonance peaks of *st*-PMMA and also a broad, weak resonance peak of the C=C backbone from 5.0 – 5.5 ppm, verifying the successful synthesis of the targeted bottlebrush polymer. Furthermore, the degree of syndiotacticity of *st*-PMMA-BB was evaluated *via* ¹³C NMR spectroscopic analysis, and found to be identical to the macromonomer ($rr = 74\%$).

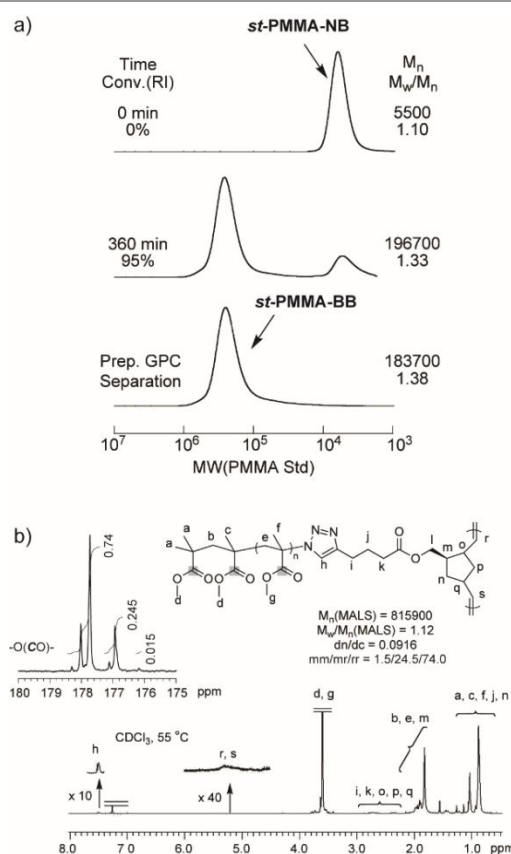


Figure 1. (a) GPC DRI traces for norbornene chain end-functionalized syndiotactic poly(methyl methacrylate) (*st*-PMMA-NB), and syndiotactic poly(methyl methacrylate) bottlebrush polymer (*st*-PMMA-BB) before and after preparative GPC purification, and (b) ¹H NMR spectrum of *st*-PMMA-BB. Inset: ¹³C NMR spectrum of carbonyl carbons.

The complexation of *st*-PMMA-BB and C₆₀ was then performed in acetonitrile (MeCN) – an excellent complexing solvent¹³ in which C₆₀ is completely insoluble^{4b} to yield the stereocomplex *st*-PMMA/C₆₀ SC. In specific solvents (like MeCN), the stereoregularity allows the *st*-PMMA side-chains of the bottlebrush polymer to re-arrange into single-stranded helical conformations. Internal cavities of these helices are thus able to accommodate C₆₀ molecules through inclusion complex formation (Scheme 1).^{8a,b} It was anticipated that the C₆₀-incorporated side-chains would cause chain-folding of *st*-PMMA-BB and finally resulting in a spherical nanoparticle, i.e. FPN, whereas uncomplexed, free polymer side-chains help stabilize the core domain and prevent intermolecular

aggregation of the nanoparticle.¹⁴ Both DLS and TEM (Figure 2a and b, respectively) analysis clearly demonstrated a substantial increase in particle size increase after complexation. The average hydrodynamic diameter (D_H) increased from 10.8 to 44.6 nm (Figure 2a and S2), and similarly, the average particle diameter measured from TEM micrographs (D_{TEM}) increased from 17.9 to 32.9 nm (Figure 2b and S3). The changes in particle size implied the successfully encapsulation of C_{60} by the **st-PMMA-BB**.

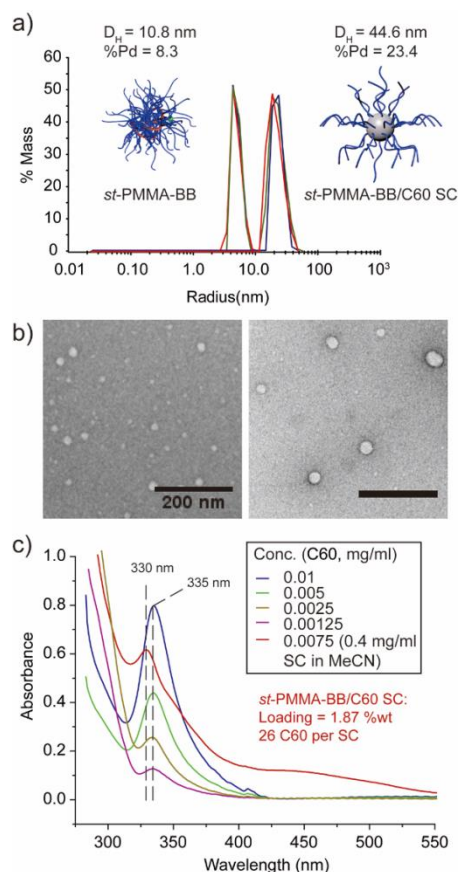


Figure 2. (a) DLS particle size distributions of the bottlebrush polymer and stereocomplex. (b) TEM images of **st-PMMA-BB** (left) and **st-PMMA-BB/C60 SC** (right). Scale bars are 200 nm. (c) UV-Vis spectrum of **st-PMMA-BB/C60 SC** (in MeCN) and calibration spectra of C_{60} (in toluene) at various concentrations.

UV-Vis spectrum of **st-PMMA/C60 SC** in MeCN solution showed the characteristic absorption peak of C_{60} at $\lambda = 330$ nm. This result showed that **st-PMMA-BB** was able to endow fullerene with solubility in polar solvents such as MeCN, and further proved the inclusion complexation of C_{60} into **st-PMMA-BB**. X-ray powder diffraction XRD was also used to characterize the isolated FPN, however, no discernable diffraction peak was observed. This is because the surrounding uncomplexed **st-PMMA** chains prevent the complexed **st-PMMA/C60** core of the nanoparticles from forming crystallite domains *via* inter-particle aggregation. This can be verified by both DLS and TEM particle size plots of the **st-PMMA/C60 SC** that showed monomodal distributions with low values of percentage standard deviations (% dispersity = 23.4 and 20.5 from DLS and TEM analysis, respectively), suggesting no or minimal particle aggregation. Using the previously established UV-Vis calibration method,^{13a} the amount of encapsulated C_{60}

was determined to be 1.6 wt% of the total nanoparticle, which is equivalent to 26 C_{60} molecules per bottlebrush polymer (Figure 2c and Figure S4). The degree of inclusion complexation judging from the C_{60} content was lower than that of the previously reported system by Kawauchi *et al.* (5.8 wt%) under the same reaction conditions.^{13a} However, the previous system utilized anionically polymerized linear **st-PMMA** with higher stereoregularity ($M_n = 322$ kDa, $\bar{D} = 1.29$, $mm/mr/rr$ (%) = 0/6/94) as the polymer precursor. A higher degree of syndiotacticity means smaller amounts of irregular **st-PMMA** helical sequences that cannot participate in inclusion complexation, and therefore higher C_{60} loading. In addition, the architecture of the bottlebrush polymer means that the **st-PMMA** brushes may be too sterically hindered for higher degree of complexation with C_{60} molecules. It must be emphasized, however, that this study provides a novel C_{60} nanocarrier (i.e., **st-PMMA-BB**) that employs less demanding, more accessible chemistries (i.e., SLRP and 'click' reaction) compared to living anionic polymerization.

For organic solar cells, the electrical contact between inorganic electrode and organic active layer is a critical factor for the fabrication of efficient photovoltaic devices.¹⁵ Recently, it was reported that ultra-thin fullerene derivative interlayers on the metal oxide surfaces enhanced the photovoltaic device performance significantly due to efficient charge extraction.¹⁶ We wanted to see if device enhancement can be observed if the **st-PMMA/C60 SC** was used in a similar fashion. Polymer solar cells with inverted device geometry was fabricated with a ZnO nanoparticle interlayer and polymer:PCBM blend as the active layer (Figure 3b). Three interlayer structures were examined and compared: i) ZnO only; ii) **st-PMMA-BB** on ZnO; and iii) **st-PMMA/C60 SC** on ZnO. The current density-voltage data for the devices containing P3HT:PC₆₁BM 1:1 active layer are shown in Figure 3c.

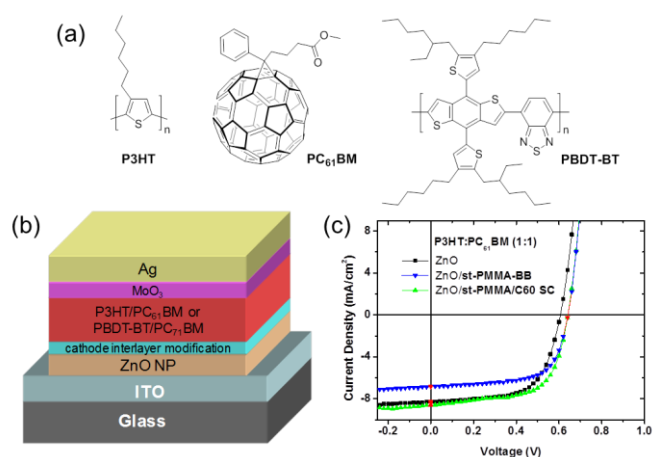


Figure 3. (a) Molecular structure of P3HT, PC₆₁BM and PBDBT-BT; (b) Schematic diagram inverted device geometry of polymer solar cell with 3 cathode interlayer variation tested – ZnO only, ZnO/**st-PMMA-BB** and ZnO/**st-PMMA-C60 SC**; and (c) J-V curves of P3HT:PC₆₁BM based BHJ solar cells.

The device performance characteristics are summarized in Table 1. The control device with ZnO interlayer showed a short-circuit current density (J_{sc}) of 8.3 mAcm⁻², an open-circuit voltage (V_{oc}) of 0.60 V, a fill factor (FF) of 64% and a

corresponding PCE of 3.21%. With **st-PMMA/C60 SC** layer, both V_{oc} and J_{sc} slightly increased resulting in the enhancement of PCE to 3.6%. Since the open-circuit voltage of an OSC is determined by the work function difference between the two electrodes, here, the enhancement of V_{oc} can be attributed to the reduced work function of cathode electrode due to surface passivation of ZnO layer.¹⁷ Pleasingly, the polymer interlayer without C₆₀, i.e. **st-PMMA-BB**, led to a slight decrease in device performance primarily as a result of smaller J_{sc} . This can be attributed to the fact that **st-PMMA-BB** is an electrically insulating material and is not expected to promote charge extraction.

Table 1. Photovoltaic device performance of polymer solar cells with various cathode interlayers.

Active layer	Cathode Interlayer	J_{sc} (mA/cm ²)	V_{oc} (V)	FF (%)	PCE (%)
P3HT: PC ₆₁ BM	ZnO	8.30	0.60	64	3.20 (3.1±0.10)
	ZnO/st-PMMA-BB	6.85	0.64	65	2.95 (2.8±0.15)
	ZnO/st-PMMA-C60	8.60	0.64	65	3.60 (3.4±0.20)
PBDT-BT: PC ₇₁ BM	ZnO	11.6	0.88	44	4.70 (4.5±0.20)
	ZnO/st-PMMA-BB	10.7	0.90	49	4.75 (4.6±0.15)
	ZnO/st-PMMA-C60	13.5	0.90	50	6.1 (6.0±0.10)

In addition to P3HT:PCBM active layer, we have also studied the effect of **st-PMMA-BB** and **st-PMMA/C60 SC** interlayers using a donor-acceptor polymer PBDT-BT (Figure 3a) and PC₇₁BM blend as active layer in inverted device geometry (Table 1, Figure S5). **As observed with P3HT-based photovoltaic device, PBDT-BT-based solar cells showed enhanced performance (PCE of 6.1%) with st-PMMA/C60 SC interlayer compared to devices with ZnO layer only.** As with the P3HT/PC₆₁BM devices, the enhanced performance can be attributed to the suppression of charge recombination at the interface due to surface passivation of ZnO layer.¹⁷ **From Table 1, it can be observed that the enhancement in device performance of PBDT-BT solar cells was higher compared to P3HT devices, which might be due to the difference in vertical morphology of the active layer.**¹⁸ The surface morphology of the interlayers were examined using atomic force microscopy AFM (Figure S6). Interestingly, the **st-PMMA/C60 SC** nanoparticles observed in the TEM experiment (Figure 2b) was also apparent in the AFM experiment.

In conclusion, a syndiotactic PMMA bottlebrush polymer material **st-PMMA-BB** was synthesized. This polymer assembled into nanoparticle structures when complexed with C₆₀ in favourable solvent systems. The polymer-fullerene composite **st-PMMA/C60 SC** was used as the electrode interlayer in polymer solar cells leading to enhancements in device performance.

This work was initiated through the Melbourne Materials Institute Seed Funding program (W.W.H.W and E.H.H.W.) and

was partly supported by funds from the Australian Renewable Energy Agency through the Australian Centre for Advanced Photovoltaics. W.W.H.W. is supported by an Australian Research Council Future Fellowship (FT130100500). Responsibility for the views, information, or advice herein is not accepted by the Australian Government.

References

- R. Søndergaard, M. Hösel, D. Angmo, T. T. Larsen-Olsen and F. C. Krebs, *Mater. Today*, 2012, **15**, 36
- L. Echegoyen and L. E. Echegoyen, *Acc. Chem. Res.*, 1998, **31**, 593.
- P. J. Bracher and D. I. Schuster, in *Fullerenes: From Synthesis to Optoelectronic Properties*, eds. D. Guldi and N. Martin, Springer Netherlands, 2002, pp. 163-212.
- (a) P. A. Troshin, H. Hoppe, J. Renz, M. Egginger, J. Y. Mayorova, A. E. Goryachev, A. S. Peregodov, R. N. Lyubovskaya, G. Gobsch, N. S. Sariciftci and V. F. Razumov, *Adv. Funct. Mater.*, 2009, **19**, 779; (b) R. S. Ruoff, D. S. Tse, R. Malhotra and D. C. Lorents, *J. Phys. Chem.*, 1993, **97**, 3379.
- M. C. Scharber, D. Mühlbacher, M. Koppe, P. Denk, C. Waldauf, A. J. Heeger and C. J. Brabec, *Adv. Mater.*, 2006, **18**, 789.
- C.-Z. Li, H.-L. Yip and A. K. Y. Jen, *J. Mater. Chem.*, 2012, **22**, 4161.
- (a) S. Qi, H. Iida, L. Liu, S. Irle, W. Hu and E. Yashima, *Angew. Chem. Int. Ed.*, 2013, **52**, 1049; (b) T. Kawauchi, A. Kitaura, M. Kawauchi, T. Takeichi, J. Kumaki, H. Iida and E. Yashima, *J. Am. Chem. Soc.*, 2010, **132**, 12191.
- (a) T. Kawauchi, J. Kumaki, A. Kitaura, K. Okoshi, H. Kusanagi, K. Kobayashi, T. Sugai, H. Shinohara and E. Yashima, *Angew. Chem. Int. Ed.*, 2008, **47**, 515; (b) T. Kawauchi, A. Kitaura, J. Kumaki, H. Kusanagi and E. Yashima, *J. Am. Chem. Soc.*, 2008, **130**, 11889; (c) J. M. Ren, K. Satoh, T. K. Goh, A. Blencowe, K. Nagai, K. Ishitake, A. J. Christofferson, G. Yiapanis, I. Yarovsky, M. Kamigaito and G. G. Qiao, *Angew. Chem. Int. Ed.*, 2014, **53**, 459; (d) T. K. Goh, J. F. Tan, S. N. Guntari, K. Satoh, A. Blencowe, M. Kamigaito and G. G. Qiao, *Angew. Chem. Int. Ed.*, 2009, **48**, 8707.
- (a) Y. Xia, J. A. Kornfield and R. H. Grubbs, *Macromolecules*, 2009, **42**, 3761; (b) Y. Xia, B. D. Olsen, J. A. Kornfield and R. H. Grubbs, *J. Am. Chem. Soc.*, 2009, **131**, 18525.
- (a) K. Satoh and M. Kamigaito, *Chem. Rev.*, 2009, **109**, 5120; (b) T. Shibata, K. Satoh, M. Kamigaito and Y. Okamoto, *J. Polym. Sci. Polym. Chem.*, 2006, **44**, 3609.
- (a) Z. Li, K. Zhang, J. Ma, C. Cheng and K. L. Wooley, *J. Polym. Sci. Polym. Chem.*, 2009, **47**, 5557; (b) S. Jha, S. Dutta and N. B. Bowden, *Macromolecules*, 2004, **37**, 4365.
- S. S. Sheiko, B. S. Sumerlin and K. Matyjaszewski, *Progress Polym. Sci.*, 2008, **33**, 759.
- (a) M. Kawauchi, T. Kawauchi and T. Takeichi, *Macromolecules*, 2009, **42**, 6136; (b) J. Špěváček, B. Schneider, *Adv. Colloid Interface Sci.* 1987, **27**, 81; (c) K. te Nijenhuis, in *Poly(vinyl methacrylate) Thermoreversible Networks*, Springer Berlin, 1997, pp. 67.
- J. M. Ren, K. Ishitake, K. Satoh, A. Blencowe, Q. Fu, E. H. H. Wong, M. Kamigaito and G. G. Qiao, *Macromolecules*, 2016, DOI: 10.1021/acs.macromol.5b02295.
- (a) T.-H. Lai, S.-W. Tsang, J. R. Manders, S. Chen and F. So, *Mater. Today*, 2013, **16**, 424; (b) E. L. Ratcliff, B. Zacher and N. R. Armstrong, *J. Phys. Chem. Lett.*, 2011, **2**, 1337; (c) L.-M. Chen, Z. Xu, Z. Hong and Y. Yang, *J. Mater. Chem.*, 2010, **20**, 2575.
- (a) S.-H. Liao, H.-J. Jhuo, Y.-S. Cheng and S.-A. Chen, *Adv. Mater.*, 2013, **25**, 4766; (b) J. Subbiah, B. Purushothaman, M. Chen, T. Qin, M. Gao, D. Vak, F. H. Scholes, X. Chen, S. E. Watkins, G. J. Wilson, A. B. Holmes, W. W. H. Wong and D. J. Jones, *Adv. Mater.*, 2015, **27**, 702.
- (a) J. Subbiah, D. Y. Kim, M. Hartel and F. So, *Appl. Phys. Lett.*, 2010, **96**, 063303; (b) Y. E. Ha, M. Y. Jo, J. Park, Y.-C. Kang, S. I. Yoo and J. H. Kim, *J. Phys. Chem. C*, 2013, **117**, 2646.
- (a) Z. Xu, L.-M. Chen, G. Yang, C.-H. Huang, J. Hou, Y. Wu, G. Li, C.-S. Hsu and Y. Yang, *Adv. Funct. Mater.*, 2009, **19**, 1227; (b) J. Subbiah, C. Amb, Irfan, Y. Gao, J. R. Reynolds and F. So, *ACS Appl. Mater. Interfaces*, 2012, **4**, 866.